Flexibility management with virtual batteries of thermostatically controlled loads: real-time control system and potential in Spain

Alejandro Martín-Crespo [1,*] ⓘ **, Sergio Saludes-Rodil** [1,] ⓘ **and Enrique Baeyens** [2,] ⓘ

1   Centro Tecnológico CARTIF, Parque Tecnológico de Boecillo 305, Boecillo, Valladolid, Spain; sersal@cartif.es
2   Instituto de las Tecnologías Avanzadas de la Producción, Universidad de Valladolid, Paseo del cauce 59, Valladolid, Spain; enrbae@eii.uva.es
*   Correspondence: alemar@cartif.es; Tel.: +34 983 546 504

Abstract: Load flexibility management is a promising approach to face the problem of balancing generation and demand in electrical grids. This problem is becoming increasingly difficult due to the variability of renewable energies. Thermostatically controlled loads can be aggregated and managed by a virtual battery, and they provide a cost-effective and efficient alternative to physical storage systems to mitigate the inherent variability of renewable energy sources. But virtual batteries require of an accurate control system being capable of tracking frequency regulation signals with minimal error. A real-time control system allowing virtual batteries to accurately track frequency or power signals is developed. The performance of this controller is validated for a virtual battery composed of 1,000 thermostatically controlled loads. Using virtual batteries equipped with the developed controller, a study focused on residential thermostatically controlled loads in Spain is performed. The results of the study quantify the potential of this technology in a country with different climate areas and provides insight about the feasibility of virtual batteries as enablers of electrical systems with high levels of penetration of renewable energy sources.

Keywords: Virtual battery, Thermostatically controlled loads, Demand side management, Frequency regulation, Spain.

1. Introduction

A sustainable and environmentally friendly electric system requires increasing the generation of energy coming from renewable sources, such as solar and wind energy. The higher penetration of renewable energy sources in the electric system reduces emissions of greenhouse gases and pollutants. However, this type of energy is uncertain and intermittent, and therefore not completely predictable. Consequently, the task of balancing electricity demand and generation is becoming more complicated. As the penetration of renewable energy sources grows, more advanced and efficient regulation strategies are required to balance the power of the system. In this scenario, flexibility management (FM) could become a suitable cost-effective alternative to overcome these technical difficulties.

Nowadays, an increasing number of houses have electric appliances that exploit their own thermal inertia, or that of the home, for their operation. These appliances are called "thermostatically controlled loads" (TCLs), and they are important FM resources. Their operation can be controlled in order to provide frequency regulation to the electrical grid, while respecting their own physical constraints and the user requirements. TCLs are also available in many industrial processes. Some examples are cold rooms and certain chemical reactors. In order to promote their operation as balancing resources for distribution system operators, TCLs can be aggregated into virtual batteries (VBs). Likewise conventional batteries, they are defined in terms of global quantities such as capacity, state of charge (SOC) and power, but with some differences, as it is explained later in this paper. Several studies characterize VBs

involving homogeneous or heterogeneous TCLs [1–6]. The last one is closer to the real-world, and has a greater significance and a broader application possibilities.

The main contribution of this paper is a study about the potential of VBs enabled by residential TCLs in Spain. Similar studies have been carried out in other countries and regions, such as Denmark, [7], Germany, [8], Great Britain, [9], Switzerland [10], California, [11] and Sardinia, [12]. But, to the best of our knowledge, this is the first one applied to Spain. In all the abovementioned studies, authors found that TCLs can provide huge potential to mitigate the negative effects of the increase in renewable energy sources in the electrical system. The current study for the Spanish case considers three different climate areas [13], featuring different prevalent weather conditions that may affect the renewable energy generation potential and TCLs performance. In order to fully understand the potential impact of the VBs in Spain, an accurate real-time VB control system has been developed and validated by simulation. The control set-point is determined by the grid operator, who determines the power required at every time instant based on the grid status.

Flexible loads, such as electrical vehicles (EVs) or TCLs, have been extensively studied as elements that could be aggregated to act as a virtual battery [14–16]. A theoretical characterization of the aggregate power and energy capacities for a collection of TCLs is reported in [3], as well as a priority-stack-based control strategy for frequency regulation using TCLs. A generalized battery model that can be directly controlled by an aggregator is introduced in [17]. The two abovementioned papers establish a TCL behaviour model and a VB control system. A study that experimentally models VBs is reported in [18], where a first-order model is adjusted using binary search algorithms. The operating reserve provided by an aggregation of heterogeneous TCLs can also be modelled probabilistically, as explained in [19–23], using Markov chains, as in [24–26], or applying model predictive control [27,28]. Several of these papers do not take into account the real short-term instantaneous status of TCLs, and some of them are focused on changing the set-point temperature of the devices, which could imply reducing users' comfort. In [29], a stochastic battery model along with a control system which performs TCLs monitoring tasks is proposed, although frequent data acquisition is performed, the system does not accurately fit the grid requirements.

In [30], the technical viability of frequency regulation by TCLs is analysed, and it is proved that the load contribution can be significant. These thermal devices can also be applied to voltage control. [31]. TCLs are useful in microgrids, as explained in [32], and in virtual energy storage systems (VESS) [33], where their capability to provide ancillary services is studied. Another use of TCLs is the management of intraday wholesale energy market prices [34].

The remainder of this paper is organised as follows. In Section 2, models of an individual TCL and a VB are introduced. These models are used to develop a new VB control system that improves the accuracy in power delivery as compared to previously designed control systems. In Section 3, our control systems are used to study the capabilities of VBs as a cost-effective solution to balance power generation and consumption in electric systems with a large penetration of renewable energy sources. The study is carried out for residential TCLs in Spain. Section 4 shows and discuss the results of the study. Previously, the performance of the new VB control system is validated through simulated experiments. Finally, the conclusion is given in Section 5.

2. The Virtual Battery

A VB is defined as an aggregated collection of TCLs operated by a suitable control system to provide power and frequency regulation to the electrical grid. VBs are combined with adequate regulation policies to increase penetration of renewable energy generation sources in the grid by balancing power demand and generation in a cost-effective manner.

Symbol	Meaning
θ	TCL temperature (°C)
$\hat{\theta}_a$	Forecast ambient temperature (°C)
θ_s	Set point temperature (°C)
Δ	Temperature dead-band (°C)
ω	Perturbation (°C)
R_{th}	Thermal resistance (°C/kW)
C_{th}	Thermal capacity (kWh/°C)
P	Nameplate power (kW)
P_0	Mean power (kW)
η	Coefficient of performance
ϕ	Kind of device
u	Status
δ	Availability
γ	Full availability
λ	Time to reach bound temperature (h)
ζ	Cycle elapsed time (h)
κ	Minimum cycle elapsed time (h)

Table 1: TCL parameters

A new real-time VB control system, which accurately follows the operator signal, is developed in this section. The control strategy complies with users and device constraints, such as TCL temperature bounds or short-cycling prevention. The goal is achieved by anticipating variations imposed by the abovementioned constraints. Our control strategy is an improvement of that reported in [35].

The models of TCL and VB used to develop the new control system are explained below. They quantify the stored energy and the maximum power the VB may provide. The models are represented in discrete-time and the sampling time is denoted by h.

2.1. The TCL model

A model allows the controller to predict the behavior of each TCL and estimate its stored energy. The parameters describing a TCL are collected in Table 1. The nameplate power P_i is a positive quantity in cooling devices and negative in heating devices. The typical values of these parameters for residential TCLs are shown in Table 2. Reversible heat pumps are classified into two different types: 'reversible heat pumps (heat)' and 'reversible heat pumps (cold)'. The motivation for this classification is that some reversible heat pumps are only used for heating or cooling, not for both tasks. Besides, they have a different operation mode in the VB control algorithm.

Several discrete-time models of a TCL have been proposed in the literature [3,29]. Here, we use the model given in [29] because it is more realistic with a small cost of increasing complexity. In this model, the temperature θ_i of each TCL i is calculated for every time instant k using the following equation

$$\theta_i^{k+1} = g_i \theta_i^k + (1 - g_i)(\hat{\theta}_{a_i}^k - u_i^k \theta_{g_i}) + \omega_i^k, \tag{1}$$

where

$$g_i = e^{-1/R_{th_i} C_{th_i}}, \quad \theta_{g_i} = R_{th_i} P_i \eta_i. \tag{2}$$

Each TCL has a set-point temperature (θ_{s_i}), which is set by the user, and a temperature dead-band (Δ_i) determined by the design of the TCL or by the user. Both parameters define

TCL	R_{th} (°C/kW)	C_{th} (kWh/°C)	P (kW)	η	θ_s (°C)	Δ (°C)
Reversible heat pump (heat)	$1.5 - 2.5$	$1.5 - 2.5$	$(-4) - (-7.2)$	3.5	$15 - 24$	$0.25 - 1.0$
Reversible heat pump (cold)	$1.5 - 2.5$	$1.5 - 2.5$	$4 - 7.2$	2.5	$18 - 27$	$0.25 - 1.0$
Non-reversible heat pump	$1.5 - 2.5$	$1.5 - 2.5$	$(-4) - (-7.2)$	3.5	$15 - 24$	$0.25 - 1.0$
Cold pump	$1.5 - 2.5$	$1.5 - 2.5$	$4 - 7.2$	2.5	$18 - 27$	$0.25 - 1.0$
Electric water heater	$100 - 140$	$0.2 - 0.6$	$(-4) - (-5)$	1	$43 - 54$	$2 - 4$
Refrigerator	$80 - 100$	$0.4 - 0.8$	$0.1 - 0.5$	2	$1.7 - 3.3$	$1 - 2$

Table 2: Range of values for the parameters of residential TCLs [36]

the comfort band, whose bounds are $\theta_{s_i} \pm \Delta_i$. The temperature θ_i must always be inside this comfort band.

Consequently, the control system aims to maintain the temperature θ_i in the comfort band. The average power to get the objective (P_{0_i}) is given by

$$P_{0_i}^k = \frac{\hat{\theta}_{a_i}^k - \theta_{s_i}}{\eta_i R_{th_i}}. \tag{3}$$

In order to maintain the temperature in the comfort band, each load can be switched on and off by the control system depending on the temperature and its own status.

Each device is characterized by four binary-valued variables: device type (ϕ_i), status (u_i), availability (δ_i) and total availability (γ_i). The device type ϕ_i is 0 for a cooling TCL and 1 for a heating TCL. The device status u_i is 1 when it is working, *i.e.*, the motor is on with fixed power consumption P_i, and 0 when off, with zero power consumption. The device availability δ_i is 1 when the TCL is available for the control system and 0 otherwise. A TCL is available when θ_i lies within the comfort band, and the time elapsed after its last change of status is large enough to avoid short-cycling. The full availability of the device γ_i is 0 when the ambient forecast temperature $\hat{\theta}_{a_i}$ is lower (in cooling devices) or higher (in heating devices) than any TCL temperature bound. This last parameter indicates whether the TCL is ready to operate or not.

Short-cycling has harmful effects for electrical TCL systems. It causes damage in the electromechanical components, decreases their expected lifetime and can also significantly drive up the energy consumption. In order to avoid short-cycling, a minimum cycle elapsed time κ_i is defined. Let ζ_i be the elapsed time after the last status change, then the TCL device is available if $\theta_i \in [\theta_{s_i} - \Delta_i, \theta_{s_i} + \Delta_i]$ and $\zeta_i > \kappa_i$.

The time to reach the temperature bound (λ_i) is the time that a TCL can be off without reaching that bound. It is calculated by simulating the evolution of θ_i over time using the TCL dynamic model given by (1). If the TCL is not available, *i.e.* if $\delta_i = 0$, then λ_i also equals 0.

2.2. The VB model

The VB model is an abstraction that represents a large number of TCLs with a reduced number of parameters. It allows the grid operator to make decisions in order to efficiently manage the grid. The set of parameters that describe a VB is given in Table 3.

The capacity of the VB is represented by two different parameters, C_c and C_d, to model the lack of symmetry in the dynamics of the charging and discharging processes of a TCL. In one case, the temperature change is forced by mechanical or electrical components (increasing θ in heating devices or reducing it in cooling ones), and in the other case it is not. Likewise, the state of charge (SOC_c and SOC_d), the maximum power (n_+ and n_-), and the maximum available power (n'_+ and n'_-) are also duplicated.

Symbol	Meaning
$\mathcal{N}$	Set of TCLs with cardinality N
C_c / C_d	Charging/Discharging capacity (kWh)
SOC_c / SOC_d	Charging/Discharging state of charge (kWh)
n_+ / n_-	Maximum charging/discharging power (kW)
n'_+ / n'_-	Maximum available charging/discharging power (kW)

Table 3: VB parameters

The charging capacity (C_c) is the maximum energy that can be used from every TCL $i \in \mathcal{N}$ whose status u_i is 1. If the VB is charging, then the charging state of charge (SOC_c) is the current energy reserve of the VB for charging. Likewise, the discharging capacity (C_d) and the discharging state of charge (SOC_d) represent the maximum energy that can be used for discharging and the current energy reserve for discharging. The capacities C_c and C_d are calculated by using the models to obtain the time that total available TCLs (*i.e.*, $\{i \in \mathcal{N} : \gamma_i = 1\}$) take to evolve from one temperature bound to the other. The states of charge SOC_c and SOC_d also use the TLC models, but operating from the actual temperature θ_i to the corresponding temperature bound. The algorithms developed for computing the capacities and states of charge require long-term temperature forecasts $\hat{\theta}_{a_i}$ to produce accurate results. Accurate forecasts are assumed to be available in this paper.

The maximum charging power (n_+) is the maximum power a VB can provide for charging, assuming that all TCLs are available (δ_i is 1):

$$n_+^{k+1} = \sum_{i=1}^{N}(1 - 2\phi_i)(P_i - P_{0_i}^k). \tag{4}$$

The maximum available charging power (n'_+) is the maximum power that a VB can provide in the following instant, considering only the available TCLs. It is calculated by excluding the TCLs that are unavailable for charging:

$$(n'_+)^{k+1} = n_+^{k+1} - P_+^k, \tag{5}$$

where P_+ is the sum of power of the TCLs which are unavailable for charging. TCLs are unavailable for charging when their status cannot be on in the next time instant.

The maximum available discharging power (n_-) is the same as n_+, but for the discharging process:

$$n_-^{k+1} = \sum_{i=1}^{N}(1 - 2\phi_i)(P_{0_i}^k). \tag{6}$$

The maximum available discharging power (n'_-) excludes the power of the TCLs which are unavailable

$$(n'_-)^{k+1} = n_-^{k+1} - P_-^k, \tag{7}$$

where P_- is the sum of power of TCLs that are unavailable for discharging. TCLs are unavailable for discharging when their status cannot be off in the following instant.

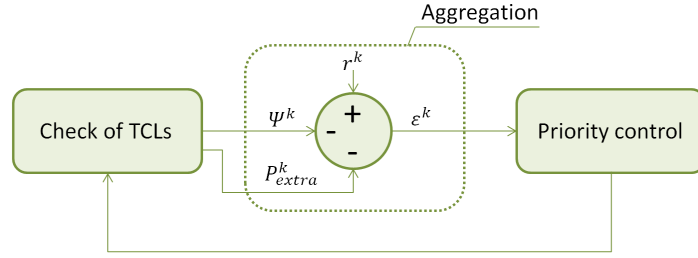The maximum powers n_+, n_-, n'_+ and n'_- are calculated considering only TCLs that are totally available (γ_i is 1).

Figure 1. Structure of the VB controller

Symbol	Meaning
P_{extra}	Extra power (kW)
r	System operator signal (kW)
P_{agg}	Aggregated power (kW)
P_{base}	Base power (kW)
ψ	System deviation (kW)
ϵ	Regulation signal (kW)
p	Power switched (kW)

Table 4: VB controller variables

2.3. The VB controller

The real-time VB control algorithm is composed of three blocks: *Check of TCLs*, *Aggregation*, and *Priority Control*. The first block is executed individually by each TCL, while the others are managed by a centralised controller. The communication between TCLs and the aggregator is done by using the method explained in [37], which requires an internet connection. An accurate long-term weather forecast is required to obtain reliable results. Figure 1 shows the complete controller structure where the interconnection of the three blocks is displayed. The set of variables that are used in the control algorithm are listed in Table 4.

2.3.1. Checking of TCL

The objective of this block is to compute the variables of a TCL at the next time instant and to avoid its temperature from leaving the comfort band. The process that a TCL i executes is detailed in Algorithm 1, see the Appendix. In this algorithm, a TCL with variables that are close to violating their constraints are identified and marked, which means that δ_i and/or γ_i become 1. The powers P_+, P_- and the extra power (P_{extra}) are calculated as well. P_{extra} is the VB total power that will be switched on or off at the next time instant in order to avoid violating the TCLs constraints.

The computed variables of each TCL should be automatically communicated to the centralised controller every time instant h. If the length of the sampling time interval h is too small, then the communication system would require a high bandwidth and very expensive hardware due to the high volume of data. Notwithstanding, the variables must be sent as often as possible, so the controller may quickly correct any power deviation. In our studies, we have used $h = 10$ seconds.

2.3.2. Aggregation

In this controller block, the data obtained from each device are aggregated and compared to the system operator signal (r). This value is the amount of power that the grid operator wants to be provided. It can be either positive or negative, and has been previously determined

by the grid operator using the current grid status and information about the VB capacity, state of charge and maximum power. If r is positive, then the VB is ordered to absorb energy. It could be caused by an excess in the renewable energy production or a strong power demand fall. However, if r is negative, then the VB has to stop consuming energy. This case corresponds to a higher power demand or a lower electric generation than expected.

System deviation (ψ) is the difference between the current power consumed by the VB, and its base power. The system deviation is obtained as

$$\psi^k = P_{agg}^k - P_{base}^k,\tag{8}$$

where

$$P_{agg}^k = \sum_{i=1}^{N}(1-2\phi_i)u_i^k P_i,\tag{9}$$

$$P_{base}^k = \sum_{i=1}^{N}(1-2\phi_i)P_{0_i}^k.\tag{10}$$

As a result of the aggregation process, the regulation signal (ϵ) is given by

$$\epsilon^k = r^k - \psi^k - P_{extra}^k.\tag{11}$$

This variable will be used at the Priority Control block, and it determines the power that finally has to be provided. The aggregation block is implemented in Algorithm 2. See the Appendix.

2.3.3. Priority Control

The last block of the control system decides which TCLs change their status variables u_i in such a way that the output VB power tracks the system operator signal r. The selected TCLs must be available and its temperature be far enough from the temperature bounds. The decision making process has been implemented in Algorithm 3, see the Appendix. The variable p tracks the total power obtained during the execution of the algorithm. The process stops when the absolute value of p exceeds the absolute value of ϵ or when every TCL has been assessed. When a TCL changes its status u_i, then the cycle elapsed time ζ_i is reset. The algorithm only works properly when the requirements of the grid operator are between the previously calculated capacities and the maximum available power. In that case, the maximum error between ψ and r is the greatest P_i in the aggregation of TCLs.

3. Residential Virtual Battery Potential in Spain

The model of a VB and its control system developed in Section 2 are used here to perform studies about the implementation of residential VBs and their capabilities. The study focuses on Spain for several reasons: its great potential for renewable energy penetration in the electric grid, the presence of different climate areas, and the availability of data. The main source of information about residential TCLs in Spain is the SECH-SPAHOUSEC project [13]. It was developed by IDAE (Instituto para la Diversificación y Ahorro de la Energía), and it estimates the penetration per house of heat pumps, cold pumps, electric water heaters and refrigerators in the different climate areas of the country in 2010. A summary of that information is shown in Table 5. According to [13], Spain is geographically classified in three different climate areas: North Atlantic, Continental and Mediterranean, see Figure 2. In order to update the current number of TCLs in Spain, shown in Table 6, the variation in the number of houses between 2010 and 2019 in each climate area is considered. This information is obtained from the ECH survey (Encuesta Continua de Hogares) [38], developed by the Spanish INE (Instituto Nacional de Estadística).

TCL	North Atlantic	Continental	Mediterranean
Reversible heat pump (heat) (%)	0.0	7.9	30.5
Reversible heat pump (cold) (%)	0.3	25.9	55.4
Non-reversible heat pump (%)	1.5	0.9	0.7
Cold pump (%)	0.1	9.8	8.0
Electric water heater (%)	19.9	18.1	38.0
Refrigerator (%)	99.9	99.8	99.4

Table 5: TCLs penetration (%) in Spain in 2010 [13]

TCL	North Atlantic	Continental	Mediterranean
Reversible heat pump (heat) (#)	0	488924	3035739
Reversible heat pump (cold) (#)	7444	1611424	5508641
Non-reversible heat pump (#)	36527	56542	73960
Cold pump (#)	1329	610388	796430
Electric water heater (#)	480534	1123051	3783823
Refrigerator (#)	2414583	6200175	9890698

Table 6: Number (#) of TCLs per climate area in 2019

Figure 2. Territorial distribution of climatic zones in Spain [13]

Figure 3. System operator signal and system deviation

In the North Atlantic climate area, the deployment of cold pumps and reversible heat pumps for air conditioning is very reduced. The reason is that the temperature is not so hot in summer as in other climate areas.

Unfortunately, to the best of our knowledge, there does not exist publicly available databases concerning thermal and electrical characteristics of TCLs in Spain. Thus, the study has been performed by sampling random data from Table 2.

4. Results and discussion

In this section, two case studies are performed and the obtained results are discussed. In the first case study, the VB operation of the controller is analysed. This study demonstrates the accurate behaviour of the controller. Later, in a second case study, the residential VB charging capacity, discharging capacity, maximum charging power, and maximum discharging power of each Spain climate area are obtained along a natural year, concluding maximum power ratios and TCL contribution percentages. For this study, a VB controlled by the new developed controller has been used.

4.1. Case study: VB controller operation

The control system developed in Section 2 has been implemented in MATLAB [39] and its performance is studied for a VB of 1000 TCLs classified as follows: 125 reversible heat pumps (cold), 125 cold pumps, 125 reversible heat pumps (heat), 125 non-reversible heat pumps, 250 refrigerators and 250 electric water heaters. The parameters of each TCL have been randomly selected by using a Gaussian probability distribution centered on the mean values given in Table 2 and standard deviation 0.1. The simulation covers 200 time instants with a sampling interval h of 10 seconds, which amounts to a total of 2000 seconds. The minimum cycle elapsed time, κ, is given a value of 60 seconds. No disturbance has been considered, *i.e.* $\omega = 0$. The initial status of each TCL has also been conveniently randomized using a binary probability distribution. The estimated ambient temperature $\hat{\theta}_a$ is fixed at 20°C in case of refrigerators and electric water heaters. For the remaining TCLs, $\hat{\theta}_a$ is variable. Figures 3–8 show the obtained results.

The system deviation ψ accurately tracks the system operator power signal r most of the time. The exception is the time interval between 510 and 750 seconds, where the maximum ψ stays at the value given by n'_+, the maximum available charging power. The reason is that the grid operator established a value of r that the VB is not capable of producing as it is outside the range previously defined by n'_+ and n'_-. This situation should be avoided by taking into account the capability, SOC and power information of the VB. When the signal r

Greatest capacities and maximum powers	Value
Greatest charging capacity (kWh)	671.9
Greatest discharging capacity (kWh)	4260.7
Greatest maximum charging power (kW)	1467.2
Greatest maximum discharging power (kW)	685.7

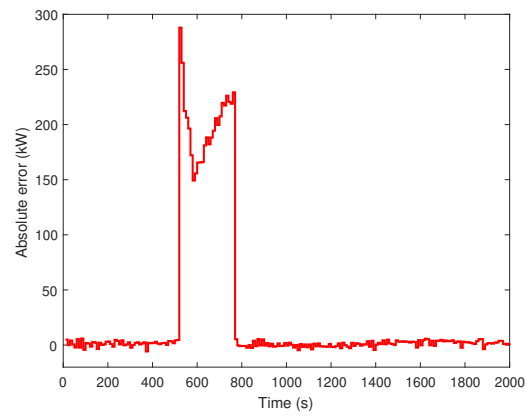Table 7: Greatest capacities and maximum powers
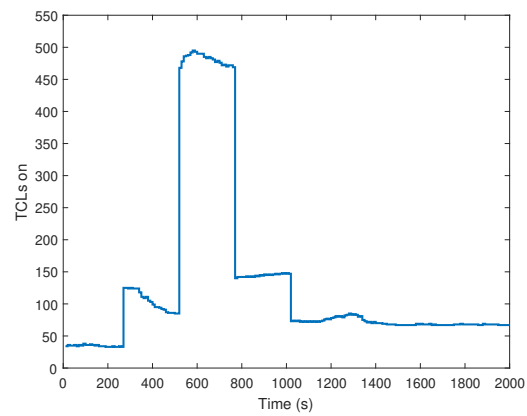

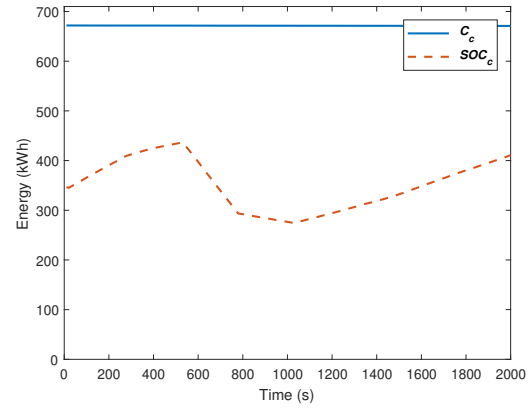**Figure 4.** Absolute error following operator signal

Figure 5. Number of TCLs on

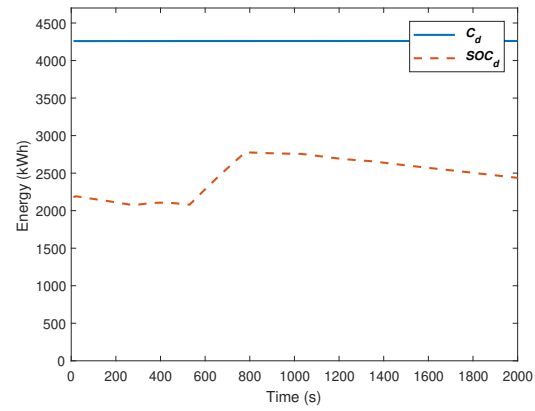**Figure 6.** Charging capacity and charging state of charge

Figure 7. Discharging capacity and discharging state of charge
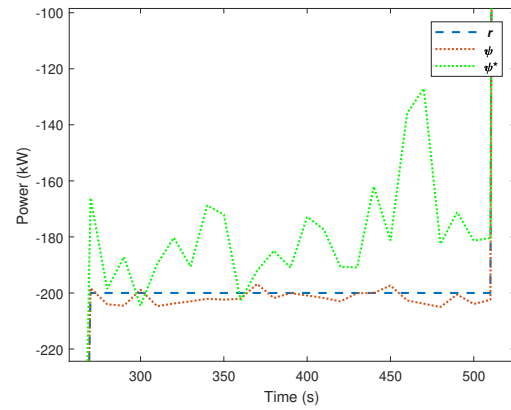

Figure 8. System deviation comparison during instants between seconds 270-510

changes, several TCLs change their status, which means that they become unavailable for 1 minute. This explains the peaks and valleys in n'_+ and n'_- when r is modified. The absolute error is lower than 6 kW in absolute value whenever r is between n'_+ and n'_-. Otherwise, the VB cannot follow the system operator signal and the absolute error is either $|r - n'_+|$ or $|n'_- - r|$. The charging/discharging capacities C_c/C_d and the maximum charging/discharging powers n_+/n_- appear to be constant in Figures 3, 6 and 7. In fact, they evolve with time but the changes are very small because the simulation time is not large enough to notice great changes in the ambient temperatures. The greatest values of these variables are given in Table 7. The charging capacity C_d is about 6.5 times greater than the discharging capacity C_c at every time instant. The reason is the lack of symmetry in the charging and discharging process, as the TCL takes more time to change its temperature θ when it is not forced to by electromechanical components, *i.e.*, when it is switched off ($u_i = 0$). Regarding the maximum charging/discharging power, n_+ is about twice as large as n_-, since the sum of the nameplate powers P_i doubles the sum of the average powers P_{0i} for every TCL $i \in \mathcal{N}$.

Figure 8 demonstrates the improvement achieved by the new controller proposed in this paper. In this figure, ψ is compared to ψ^* between the seconds 270 and 510, which is the system deviation signal when the anticipation to the variations imposed by TCLs constraints is not included in the controller. As mentioned above, ψ follows r with an absolute error not greater than an individual TCL nameplate power; while ψ^* is several times greater, as it depends on how many TCLs have to change their status forced by any of their inner constraints, which is almost random. Specifically, in this case, the maximum absolute error ψ^* becomes around 15 times as higher as the maximum absolute error ψ, in absolute value.

Besides performing short-duration regulation, the VB is able to maintain a system deviation of -300 kW for more than 15 minutes, as can be seen from time 1010 to 2000 seconds. This means that this VB can provide ancillary services to the grid similar to the primary and secondary regulation, according to the current definition given by the Spanish normative [40], which is followed by the grid operator of the country, Red Eléctrica de España. Using European Network of Transmission System Operators (ENTSO-E) terminology [41], this VB could supply regulation similar to Frequency Containment Reserves (FCR) and Frequency Restoration Reserves (FRR) services. The main difference between the regulation provided by the VB and the primary and secondary regulation is that the first acts on the demand side, whereas the others act on the generation side. As a general rule, the VB will fail to follow r earlier if the amount of power requested is larger.

4.2. Case study: VB potential in Spain

The results of the study of the VB potential in Spain are reported here. Every existing TCL in each of the three climate areas of this country are assumed be part of the corresponding VB. The charging capacity, discharging capacity, maximum charging power, and maximum discharging power of each climate area of Spain throughout a natural year are shown in Figures 10-13. The legend and colour codes for these plots are given in Figure 9. The ratios of greatest capacity and maximum power per home are shown in Table 8. Information about the contribution of each residential type of TCL to the VB potential of each climate region is collected in Tables 9–12. The average values from Table 2 for the parameters of each type of TCL have been used in the study, along with the ambient temperature of each climate area, obtained from the hourly temperature model [42] of the most populated cities in each climate area during 2019: Bilbao (North Atlantic), Madrid (Continental) and Barcelona (Mediterranean). In the case of refrigerators and electric water heaters, the ambient temperature is assumed to be constant and equal to 20°C.

Some interesting results should be highlighted. Mediterranean is the climate area with the highest VB potential, while North Atlantic has the lowest. Electric water heaters and

	North Atlantic	Continental	Mediterranean
Greatest charging capacity/home (kWh)	1.86	2.52	3.24
Greatest discharging capacity/home (kWh)	12.37	19.68	38.88
Greatest maximum charging power/home (kW)	1.13	2.93	5.29
Greatest maximum discharging power/home (kW)	0.19	1.18	1.39

Table 8: Greatest capacity and maximum power ratios per climate area in 2019

Charge capacity contribution (%)	North Atlantic	Continental	Mediterranean
Water heater	27.23	23.74	37.11
Refrigerator	72.16	69.14	51.16
Reversible heat pump (cold)	00.02	02.80	03.12
Cold pump	00.00	01.06	00.45
Reversible heat pump (heat)	00.00	02.93	07.96
Non-reversible heat pump	00.59	00.34	00.19

Table 9: Contribution percentage of each type of TCL to charging capacity per climate area in 2019

Discharging capacity contribution (%)	North Atlantic	Continental	Mediterranean
Water heater	76.17	70.85	79.73
Refrigerator	23.34	23.85	12.71
Reversible heat pump (cold)	00.02	02.34	02.35
Cold pump	00.00	00.89	00.34
Reversible heat pump (heat)	00.00	01.85	04.76
Non-reversible heat pump	00.47	00.21	00.12

Table 10: Contribution percentage of each type of TCL to discharging capacity per climate area in 2019

Maximum charging power contribution (%)	North Atlantic	Continental	Mediterranean
Water heater	76.72	51.06	50.19
Refrigerator	18.34	13.41	06.24
Reversible heat pump (cold)	00.11	13.25	10.48
Cold pump	00.02	05.02	01.51
Reversible heat pump (heat)	00.00	15.47	30.83
Non-reversible heat pump	04.81	01.79	00.75

Table 11: Contribution percentage of each type of TCL to maximum charging power per climate area in 2019

Maximum discharging power contribution (%)	North Atlantic	Continental	Mediterranean
Water heater	29.80	14.61	17.39
Refrigerator	61.29	33.01	18.60
Reversible heat pump (cold)	00.10	15.11	10.39
Cold pump	00.02	05.72	01.50
Reversible heat pump (heat)	00.00	28.28	50.88
Non-reversible heat pump	08.79	03.27	01.24

Table 12: Contribution percentage of each type of TCL to maximum discharging power per climate area in 2019
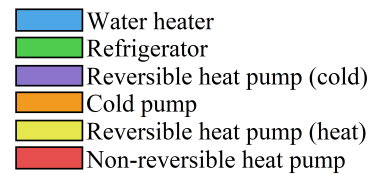
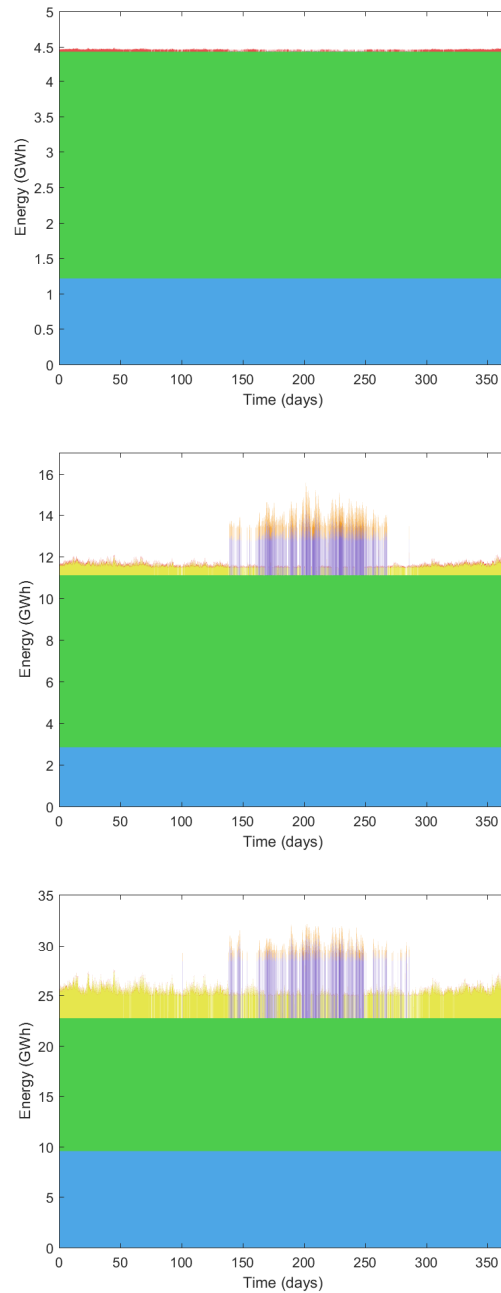**Figure 9.** Legend and colour codes for Figures 10–13

Figure 10. Charge capacity in North Atlantic, Continental and Mediterranean climate areas in 2019
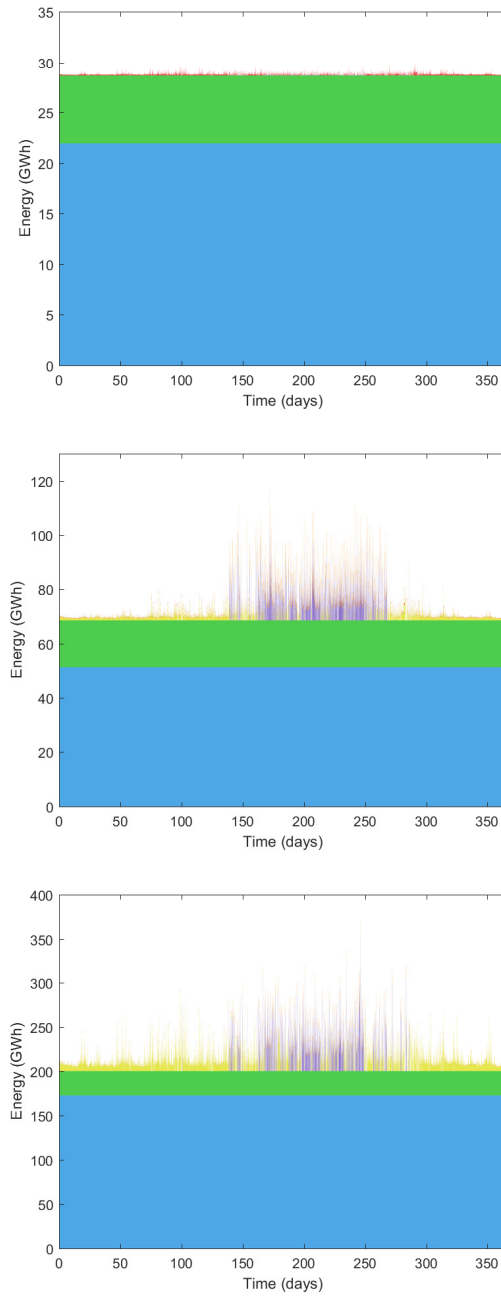
Figure 11. Discharging capacity in North Atlantic, Continental and Mediterranean climate areas in 2019
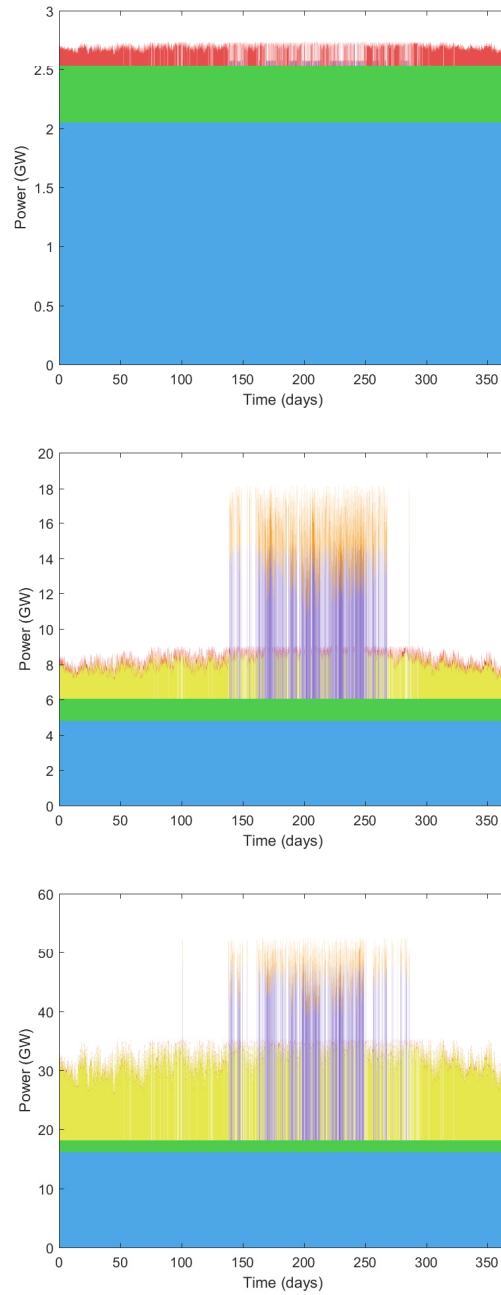
Figure 12. Maximum charging power in North Atlantic, Continental and Mediterranean climate areas in 2019
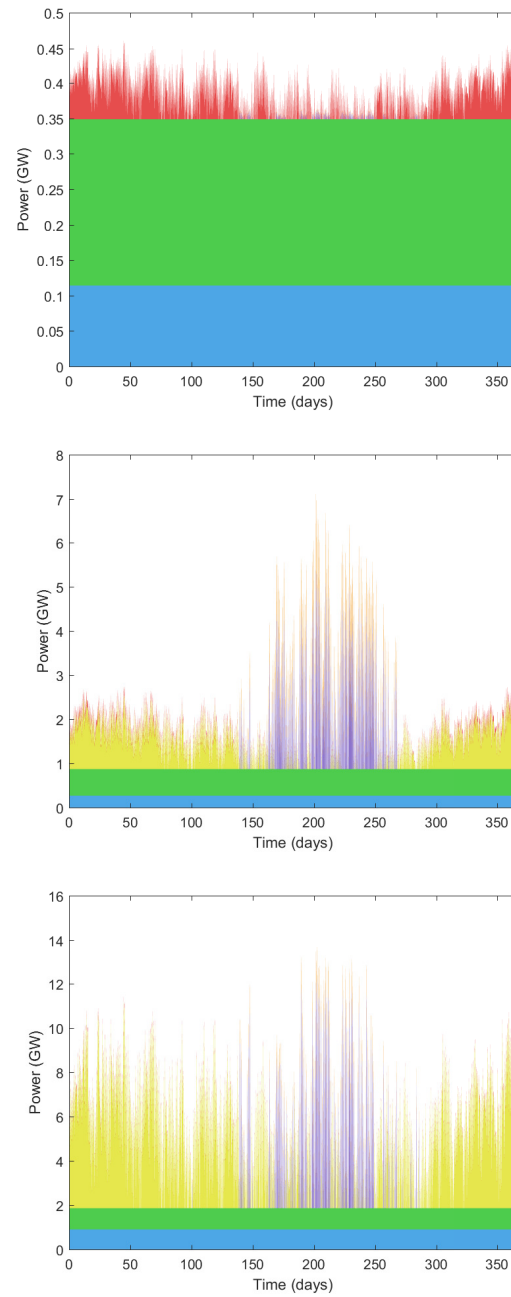
Figure 13. Maximum discharging power in North Atlantic, Continental and Mediterranean climate areas in 2019

refrigerators have the highest contribution to the charging and discharging capacity in the three climate areas. Moreover, this contribution is constant during the year, because the ambient temperature inside home is considered constant and equal to 20°C. Refrigerators have more charging capacity in every climate area, while water heaters have more discharging capacity. These constant capacities can be used for demand management at any time of the year. The remaining devices have a variable capacity contribution, as can be easily seen by the numerous peaks and valleys appearing in Figures 10–13. This is a consequence of the variability of the temperature along different hours, days and seasons. The capacity and maximum power of heat and cold pumps depend on the weather. In general, heat pumps can only be used on cold days and most of them are in winter. In contrast, cold pumps are mostly used on hot days, typically during summer. Reversible heat pumps and cold pumps have a greater contribution in Continental and Mediterranean areas than in the North Atlantic area. The reason is the greater number of them in these areas (see Table 6). Consequently, the variability in capacity and maximum power potential is more important in those climatic areas. Some summer days, the contribution of pumps to maximum charging and discharging power exceeds 50%. During these days, most of the cold pumps are working. Finally, the lack of symmetry in the charging and discharging process, explained in Section 4.1, clearly manifests here as a greater discharging capacity than charging capacity, as well as a greater maximum charging power than maximum discharging power, both for every climate area.

4.3. Discussion

A huge amount of energy and power flexibility of TCLs can be efficiently managed at real-time in a cost-effective way using a virtual battery. The control method proposed in this article to perform power regulation, control, and communication between TCLs and the aggregator improves the accuracy in tracking the system operator command power signal and does not require great investments in hardware or electronics because most of them are already installed, including the TCLs, thermal sensors and Internet connection. This is an efficient and cost-effective alternative to conventional batteries or fossil fuel solutions that require complete new installations. Furthermore, VB potential is expected to increase in the next few years due to the progressive electrification of heating devices.

Another important benefit that VBs provide is the decentralization and empowerment of consumers in the goal of balancing the grid. They become potential participants in balancing markets. Although these markets are not currently completely developed in Europe, the European Union has launched Regulation 2019/943 [43] and Directive 2019/944 [44], where balancing markets are considered. As mentioned in [43], these markets can either be individually accessed or be part of an aggregation, ensuring non-discriminatory access to all participants and respecting the need to adapt to the increasing share of variable generation and increased demand responsiveness. VBs fit properly with these requirements.

In the case of Spain, net balancing energy amounted to approximately 1209 GWh in 2019 [45]. This means an average power of 138 MW. However, positive and negative hourly peaks of more than 4000 MW are produced [46]. The study performed in this paper shows that taking advantage of FM trough VBs clearly helps to achieve power regulation goals in Spain, especially in extreme situations. The remuneration for participating in balancing markets must be important to encourage TCL owners to become contributors. Although the Mediterranean climate area has the highest residential power and capacity potential in Spain, VBs management should be profitable in any climate region if the economic profit is sufficient.

5. Conclusion

The capacity and maximum power provided by the aggregation of TCLs in Spain have been analysed in this paper. The different regions of Spain were classified into three different

climate areas and a VB including an improved real-time control has been used for this study. The obtained results show the flexibility potential of the different climate areas of the country, which should encourage power system actors to develop and implement VBs technology. In addition, a new control system for improving the operation of BV has been developed. Its performance shows excellent levels of accuracy in tracking the command signals provided by the system operator when VB constraints are fulfilled.

The results prove that VBs can be very useful in providing regulation support to electrical grids. If the communication between TCLs and aggregators is sufficiently fast, VBs becomes a cost-effective and efficient short-term energy storage alternative which, in combination with other existing ones (SMES, flywheels, etc.), greatly facilitates renewable energy penetration.

VBs are a powerful instrument for implementing demand side management programs. Their utility is closely related to the speed and reliability of communication networks, the quality of TCLs models and the prediction of the ambient temperature. Improving these aspects is driving our future research work.

Appendix A. Control Algorithms

Algorithm 1 Check of TCLs.

1: $P^k_{extra_i} = 0$
2: $P_{-_i} = 0$
3: $P_{+_i} = 0$
4: Calculate $P^{k+1}_{0_i}$
      {Total availability}
5: **if** $(\phi_i = 0$ and $\hat{\theta}^{k+1}_{a_i} < (\theta_{s_i} + \Delta_i))$ or $(\phi_i = 1$ and $\hat{\theta}^{k+1}_{a_i} > (\theta_{s_i} - \Delta_i))$ **then**
6:    $\gamma^{k+1}_i = 0, \delta^{k+1}_i = 0, u^{k+1}_i = 0$
7:    **if** $\phi_i = 0$ and $\gamma^k_i = 1$ **then**
8:        $P^k_{extra_i} = P^k_{extra_i} + P^k_{0_i}$
9:    **else if** $\phi_i = 1$ and $\gamma^k_i = 1$ **then**
10:       $P^k_{extra_i} = P^k_{extra_i} - P^k_{0_i}$
11:    **end if**
12:    **if** $\phi_i = 0$ and $u^k_i = 1$ **then**
13:        $P^k_{extra_i} = P^k_{extra_i} - P_i$
14:        $\zeta^{k+1}_i = 0$
15:    **else if** $\phi_i = 1$ and $u^k_i = 1$ **then**
16:        $P^k_{extra_i} = P^k_{extra_i} + P_i$
17:        $\zeta^{k+1}_i = 0$
18:    **end if**
19: **end if**
20: **if** $\gamma^k_i = 0$ and $\gamma^{k+1}_i = 1$ **then**
21:    **if** $\phi_i = 0$ **then**
22:        $P^k_{extra_i} = P^k_{extra_i} - P^{k+1}_{0_i}$
23:    **else if** $\phi_i = 1$ **then**
24:        $P^k_{extra_i} = P^k_{extra_i} + P^{k+1}_{0_i}$
25:    **end if**
26: **end if**
      {Forecast ambient temperature}
27: **if** $\gamma^k_i = 1$ and $\gamma^{k+1}_i = 1$ **then**
28:    **if** $\phi_i = 0$ **then**
29:        $P^k_{extra_i} = P^k_{extra_i} - P^{k+1}_{0_i} + P^k_{0_i}$
30:    **else if** $\phi_i = 1$ **then**
31:        $P^k_{extra_i} = P^k_{extra_i} + P^{k+1}_{0_i} - P^k_{0_i}$
32:    **end if**
33: **end if**
      {TCL temperature}
34: Calculate θ^{k+1}_i
35: **if** $\gamma^{k+1}_i = 1$ **then**
36:    **if** $\theta^{k+1}_i \geq (\theta_{s_i} + \Delta_i)$ **then**
37:        $\delta^{k+1}_i = 0$
38:        **if** $\phi_i = 0$ **then**
39:           $P^k_{-_i} = P^k_{-_i} + P_i$
40:           **if** $u^k_i = 0$ **then**
41:              $u^{k+1}_i = 1$
42:              $P^k_{extra_i} = P^k_{extra_i} + P_i$
43:              $\zeta^{k+1}_i = 0$
44:           **end if**

45:    **else if** $\phi_i = 1$ **then**
46:        $P^k_{+_i} = P^k_{+_i} - P_i$
47:        **if** $u^k_i = 1$ **then**
48:            $u^{k+1}_i = 0$
49:            $P^k_{extra_i} = P^k_{extra_i} + P_i$
50:            $\zeta^{k+1}_i = 0$
51:        **end if**
52:    **end if**
53:    **else if** $\theta^{k+1}_i \leq (\theta_{s_i} - \Delta_i)$ **then**
54:        $\delta^{k+1}_i = 0$
55:        **if** $\phi_i = 0$ **then**
56:            $P^k_{+_i} = P^k_{+_i} + P_i$
57:            **if** $u^k_i = 1$ **then**
58:                $u^{k+1}_i = 0$
59:                $P^k_{extra_i} = P^k_{extra_i} - P_i$
60:                $\zeta^{k+1}_i = 0$
61:            **end if**
62:        **else if** $\phi_i = 1$ **then**
63:            $P^k_{-_i} = P^k_{-_i} - P_i$
64:            **if** $u^k_i = 0$ **then**
65:                $u^{k+1}_i = 1$
66:                $P^k_{extra_i} = P^k_{extra_i} - P_i$
67:                $\zeta^{k+1}_i = 0$
68:            **end if**
69:        **end if**
70:    **end if**
71: **end if**
        {Cycled passed time}
72: **if** $\zeta^{k+1}_i \leq \kappa_i$ **then**
73:    $\delta^{k+1}_i = 0$
74:    **if** $u^{k+1}_i = 1$ and $\theta^{k+1}_i \leq \theta_{s_i} + \Delta_i$ and $\theta^{k+1}_i \geq \theta_{s_i} - \Delta_i$ and $\zeta^{k+1}_i \neq 0$ and $\gamma^{k+1}_i = 1$ **then**
75:        **if** $\phi_i = 0$ **then**
76:            $P^k_{-_i} = P^k_{-_i} + P_i$
77:        **else if** $\phi_i = 1$ **then**
78:            $P^k_{-_i} = P^k_{-_i} - P_i$
79:        **end if**
80:    **else if** $u^{k+1}_i = 0$ and $\theta^{k+1}_i \leq \theta_{s_i} + \Delta_i$ and $\theta^{k+1}_i \geq \theta_{s_i} - \Delta_i$ and $\zeta^{k+1}_i \neq 0$ and $\gamma^{k+1}_i = 1$ **then**
81:        **if** $\phi_i = 0$ **then**
82:            $P^k_{+_i} = P^k_{+_i} + P_i$
83:        **else if** $\phi_i = 1$ **then**
84:            $P^k_{+_i} = P^k_{+_i} - P_i$
85:        **end if**
86:    **end if**
87: **end if**

Algorithm 2 Aggregation.

1: $P^k_{extra} = 0$
2: **for** i from 1 to N **do**
3:     $P^k_{extra} = P^k_{extra} + P^k_{extra_i}$
4:     $P^k_+ = P^k_+ + P^k_{+_i}$
5:     $P^k_- = P^k_- + P^k_{-_i}$
6: **end for**
      {Capacity}
7: Calculate C^{k+1}_c, C^{k+1}_d
      {State of charge}
8: Calculate SOC^{k+1}_c, SOC^{k+1}_d
      {Maximum power}
9: Calculate n^{k+1}_+, n^{k+1}_-, n'^{k+1}_+, n'^{k+1}_-
      {Regulation signal}
10: Calculate P^k_{agg}, P^k_{base}, ψ^k, ϵ^k

Algorithm 3 Priority Control.

1: $p^k = 0$
   {Disaggregation}
2: **if** $\epsilon^k < 0$ **then**
3:     Calculate λ_i^k
4:     Order TCL from bigger λ_i^k to smaller λ_i^k
5:     **while** $|\epsilon^k| > |p^k|$ and $i < N$ **do**
6:         $i = i + 1$
7:         **if** $u^k = 1$ and $\delta^{k+1} = 1$ **then**
8:             $u^{k+1} = 0$
9:             $\zeta^{k+1} = 0$
10:             **if** $\phi = 0$ **then**
11:                 $p^k = p^k + P_i$
12:                 $P_+^{k+1} = P_+^{k+1} + P_i$
13:             **else if** $\phi = 1$ **then**
14:                 $p^k = p^k - P_i$
15:                 $P_+^{k+1} = P_+^{k+1} - P_i$
16:             **end if**
17:         **end if**
18:     **end while**
19: **else if** $\epsilon^k > 0$ **then**
20:     Calculate λ_i^k
21:     Order TCL from bigger λ_i^k to smaller λ_i^k
22:     **while** $|\epsilon^k| > |p^k|$ and $i < N$ **do**
23:         $i = i + 1$
24:         **if** $u^k = 0$ and $\delta^{k+1} = 1$ **then**
25:             $u^{k+1} = 1$
26:             $\zeta^{k+1} = 0$
27:             **if** $\phi = 0$ **then**
28:                 $p^k = p^k + P_i$
29:                 $P_-^{k+1} = P_-^{k+1} + P_i$
30:             **else if** $\phi = 1$ **then**
31:                 $p^k = p^k - P_i$
32:                 $P_-^{k+1} = P_-^{k+1} - P_i$
33:             **end if**
34:         **end if**
35:     **end while**
36: **end if**

References

1. Callaway, D.S.; Hiskens, I.A. Achieving Controllability of Electric Loads. *Proceedings of the IEEE* **2011**, *99*, 184–199. doi:10.1109/JPROC.2010.2081652.

2. Koch, S.; Mathieu, J.L.; Callaway, D.S. Modeling and control of aggregated heterogeneous thermostatically controlled loads for ancillary services. Proc. PSCC. Citeseer, 2011, pp. 1–7.

3. Hao, H.; Sanandaji, B.M.; Poolla, K.; Vincent, T.L. A generalized battery model of a collection of Thermostatically Controlled Loads for providing ancillary service. 2013 51st Annual Allerton Conference on Communication, Control, and Computing (Allerton), 2013, pp. 551–558. doi:10.1109/Allerton.2013.6736573.

4. Acharya, S.; El Moursi, M.S.; Al-Hinai, A. Coordinated frequency control strategy for an islanded microgrid with demand side management capability. *IEEE Transactions on Energy Conversion* **2017**, *33*, 639–651.

5. Tindemans, S.H.; Trovato, V.; Strbac, G. Decentralized control of thermostatic loads for flexible demand response. *IEEE Transactions on Control Systems Technology* **2015**, *23*, 1685–1700.

6. Wang, P.; Wu, D.; Kalsi, K. Flexibility Estimation and Control of Thermostatically Controlled Loads with Lock Time for Regulation Service. *IEEE Transactions on Smart Grid* **2020**.

7. Mathieu, J.L.; Rasmussen, T.B.; Sørensen, M.; Jòhannsson, H.; Andersson, G. Technical resource potential of non-disruptive residential demand response in Denmark. 2014 IEEE PES General Meeting | Conference Exposition, 2014, pp. 1–5. doi:10.1109/PESGM.2014.6938939.

8. Gils, H.C. Economic potential for future demand response in Germany – Modeling approach and case study. *Applied Energy* **2016**, *162*, 401 – 415. doi:https://doi.org/10.1016/j.apenergy.2015.10.083.

9. Trovato, V.; Sanz, I.M.; Chaudhuri, B.; Strbac, G. Advanced control of thermostatic loads for rapid frequency response in Great Britain. *IEEE Transactions on Power Systems* **2016**, *32*, 2106–2117.

10. Kamgarpour, M.; Vrettos, E.; Andersson, G.; Lygeros, J. Population of Thermostatically Controlled Loads for the Swiss Ancillary Service Market. Proceedings of the COLEB 2014 Workshop Computational Optimisation of Low-Energy Buildings. 6 & 7 March 2014, ETH Zürich. Citeseer, 2014, pp. 49–50.

11. Hao, H.; Sanandaji, B.M.; Poolla, K.; Vincent, T.L. Potentials and economics of residential thermal loads providing regulation reserve. *Energy Policy* **2015**, *79*, 115–126.

12. Conte, F.; Massucco, S.; Silvestro, F.; Ciapessoni, E.; Cirio, D. Stochastic modelling of aggregated thermal loads for impact analysis of demand side frequency regulation in the case of Sardinia in 2020. *International Journal of Electrical Power & Energy Systems* **2017**, *93*, 291–307.

13. Instituto para la Diversificación y ahorro de la Energía. Proyecto SHEC-SPAHOUSEC. Análisis del consumo energético del sector residencial en España. Informe final. http://www.idae.es/uploads/documentos/documentos_Informe_SPAHOUSEC_ACC_f68291 a3.pdf, 2011. [Last accessed date: 2021-02-19].

14. Han, S.; Han, S.; Sezaki, K. Estimation of achievable power capacity from plug-in electric vehicles for V2G frequency regulation: Case studies for market participation. *IEEE Transactions on Smart Grid* **2011**, *2*, 632–641.

15. Liu, H.; Hu, Z.; Song, Y.; Lin, J. Decentralized vehicle-to-grid control for primary frequency regulation considering charging demands. *IEEE Transactions on Power Systems* **2013**, *28*, 3480–3489.

16. Kempton, W.; Udo, V.; Huber, K.; Komara, K.; Letendre, S.; Baker, S.; Brunner, D.; Pearre, N. A test of vehicle-to-grid (V2G) for energy storage and frequency regulation in the PJM system. *Results from an Industry-University Research Partnership* **2008**, *32*.

17. Hao, H.; Sanandaji, B.M.; Poolla, K.; Vincent, T.L. Aggregate Flexibility of Thermostatically Controlled Loads. *IEEE Transactions on Power Systems* **2015**, *30*, 189–198. doi:10.1109/TPWRS.2014.2328865.

18. Nandanoori, S.P.; Chakraborty, I.; Ramachandran, T.; Kundu, S. Identification and Validation of Virtual Battery Model for Heterogeneous Devices. Proceedings of the IEEE Power & Energy Society General Meeting (PESGM 2019), 2019, pp. 1–5. doi:10.1109/PESGM40551.2019.8973978.

19. Ding, Y.; Cui, W.; Zhang, S.; Hui, H.; Qiu, Y.; Song, Y. Multi-state operating reserve model of aggregate thermostatically-controlled-loads for power system short-term reliability evaluation. *Applied Energy* **2019**, *241*, 46 – 58.

20. Lu, N.; Chassin, D.P.; Widergren, S.E. Modeling uncertainties in aggregated thermostatically controlled loads using a state queueing model. *IEEE Transactions on Power Systems* **2005**, *20*, 725–733.

21. Zhang, W.; Kalsi, K.; Fuller, J.; Elizondo, M.; Chassin, D. Aggregate model for heterogeneous thermostatically controlled loads with demand response. 2012 IEEE Power and Energy Society General Meeting. IEEE, 2012, pp. 1–8.

22. Perfumo, C.; Kofman, E.; Braslavsky, J.H.; Ward, J.K. Load management: Model-based control of aggregate power for populations of thermostatically controlled loads. *Energy Conversion and Management* **2012**, *55*, 36–48.

23. Kundu, S.; Sinitsyn, N.; Backhaus, S.; Hiskens, I. Modeling and control of thermostatically controlled loads. *arXiv preprint arXiv:1101.2157* **2011**.

24. Radaideh, A.; Vaidya, U.; Ajjarapu, V. Sequential Set-Point Control for Heterogeneous Thermostatically Controlled Loads Through an Extended Markov Chain Abstraction. *IEEE Transactions on Smart Grid* **2019**, *10*, 116–127. doi:10.1109/TSG.2017.2732949.

25. Mathieu, J.L.; Callaway, D.S. State estimation and control of heterogeneous thermostatically controlled loads for load following. 2012 45th Hawaii International Conference on System Sciences. IEEE, 2012, pp. 2002–2011.

26. Xia, M.; Song, Y.; Chen, Q. Hierarchical control of thermostatically controlled loads oriented smart buildings. *Applied Energy* **2019**, *254*, 113493.

27. Liu, M.; Shi, Y. Model predictive control of aggregated heterogeneous second-order thermostatically controlled loads for ancillary services. *IEEE transactions on power systems* **2015**, *31*, 1963–1971.

28. Liu, M.; Peeters, S.; Callaway, D.S.; Claessens, B.J. Trajectory tracking with an aggregation of domestic hot water heaters: Combining model-based and model-free control in a commercial deployment. *IEEE Transactions on Smart Grid* **2019**.

29. Khan, S.; Shahzad, M.; Habib, U.; Gawlik, W.; Palensky, P. Stochastic battery model for aggregation of thermostatically controlled loads. 2016 IEEE International Conference on Industrial Technology (ICIT), 2016, pp. 570–575. doi:10.1109/ICIT.2016.7474812.

30. Conte, F.; di Vergagni, M.C.; Massucco, S.; Silvestro, F.; Ciappessoni, E.; Cirio, D. Frequency Regulation by Thermostatically Controlled Loads: a Technical and Economic Analysis. 2018 IEEE Power Energy Society General Meeting (PESGM), 2018, pp. 1–5. doi:10.1109/PESGM.2018.8586247.

31. Bogodorova, T.; Vanfretti, L.; Turitsyn, K. Voltage control-based ancillary service using thermostatically controlled loads. 2016 IEEE Power and Energy Society General Meeting (PESGM). IEEE, 2016, pp. 1–5.

32. Wang, Y.; Tang, Y.; Xu, Y.; Xu, Y. A Distributed Control Scheme of Thermostatically Controlled Loads for the Building-Microgrid Community. *IEEE Transactions on Sustainable Energy* **2019**, pp. 1–1. doi:10.1109/TSTE.2019.2891072.

33. Cheng, M.; Sami, S.S.; Wu, J. Benefits of using virtual energy storage system for power system frequency response. *Applied energy* **2017**, *194*, 376–385.

34. Mathieu, J.L.; Kamgarpour, M.; Lygeros, J.; Andersson, G.; Callaway, D.S. Arbitraging intraday wholesale energy market prices with aggregations of thermostatic loads. *IEEE Transactions on Power Systems* **2014**, *30*, 763–772.

35. Martín Crespo, A.; Saludes Rodil, S. Uso de la flexibilidad de cargas eléctricas con inercia térmica mediante una batería virtual para la regulación de red. *V Congreso Smart Grids: Libro de Comunicaciones* **2018**.

36. Mathieu, J.L. Modeling, analysis, and control of demand response resources. PhD thesis, UC Berkeley, 2012.

37. Lakshmanan, V.; Marinelli, M.; Kosek, A.M.; Nørgård, P.B.; Bindner, H.W. Impact of thermostatically controlled loads' demand response activation on aggregated power: A field experiment. *Energy* **2016**, *94*, 705 – 714.

38. Instituto Nacional de Estadística. Número de hogares por provincias según tipo de hogar y número de habitaciones de la vivienda. http://www.ine.es/jaxi/Tabla.htm?path=/t20/p274/serie/def/p03/l0/&file=03003.px&L=0. [Last accessed date: 2021-02-19].

39. The Mathworks, Inc., Natick, Massachusetts. *MATLAB version 2019b*, 2019.

40. España. Resolución de 13 de julio de 2006, de la Secretaría General de Energía, por la que se aprueba el procedimiento de operación 1.5 «Establecimiento de la reserva para la regulación frecuencia-potencia». *Boletín Oficial del Estado* **2016**, *173*, 27473–27474.

41. Smart Energy Demand Coalition. Explicit Demand Response In Europe – Mapping the Markets 2017. https://www.smarten.eu/wp-content/uploads/2017/04/SEDC-Explicit-Demand-Response-in-Europe-Mapping-the-Markets-2017.pdf. [Last accessed date: 2021-02-19].

42. España. Documento Básico HE Ahorro de Energía. *Código Técnico de la Edificación* **2017**.

43. European Union. Regulation (EU) 2019/943 of the European Parliament and of the Council of 5 June 2019 on the internal market for electricity. *Official Journal of the European Union* **2019**, *L 158/154*.

44. European Union. Directive (EU) 2019/944 of the European Parliament and of the Council of 5 June 2019 on common rules for the internal market for electricity and amending Directive 2012/27/EU. *Official Journal of the European Union* **2019**, *L 158/125*.

45. Red Eléctrica de España. Net balancing energy. https://www.esios.ree.es/en/analysis/762?vis=1&start_date=01-01-2019T00%3A00&end_date=31-12-2019T23%3A50&compare_start_date=01-01-2018T00%3A00&groupby=year. [Last accessed date: 2021-02-19].

46. Red Eléctrica de España. Net balancing energy. https://www.esios.ree.es/en/analysis/762?vis=1&start_date=01-01-2019T00%3A00&end_date=31-12-2019T23%3A50&compare_start_date=01-01-2018T00%3A00&groupby=hour. [Last accessed date: 2021-02-19].